International Journal of Thermofluids 23 (2024) 100785

Contents lists available at ScienceDirect

International Journal of Thermofluids

journal homepage: www.sciencedirect.com/journal/international-journal-of-thermofluids

Advancing thermal efficiency and entropy management inside decagonal enclosure with and without hot cylindrical insertions

Jahidul Islam Jihan [a], Bijan Krishna Saha [b], Preetom Nag [c], Nur Jahangir Moon [b], Goutam Saha [d,e,*], Suvash C. Saha [e]

[a] Department of Mechanical Engineering, Hajee Mohammad Danesh Science and Technology University, Dinajpur 5200, Bangladesh
[b] Department of Mathematics, University of Barishal, Barishal 8254, Bangladesh
[c] Department of Mathematics & Physics, North South University, Dhaka 1229, Bangladesh
[d] Department of Mathematics, University of Dhaka, Dhaka 1000, Bangladesh
[e] School of Mechanical and Mechatronic Engineering, University of Technology Sydney, NSW 2007, Australia

ARTICLE INFO

Keywords:
Natural convection
Decagon cavity
Heat transfer
Entropy generation
Heated cylinder

ABSTRACT

Effective cooling mechanisms are considered advancements in thermal control systems for diverse engineering purposes. Considering this fact, this investigation explores the analysis of natural convection and entropy generation by employing a decagonal enclosure using Galerkin Residual Finite Element method. In this study, influence of Rayleigh number ($10^3 \leq Ra \leq 10^6$), Bejan number (*Be*), Prandtl number ($0.71 \leq Pr \leq 7$), and isothermal boundary condition are considered. The findings reveal that both *Ra* and *Pr* significantly impact the characteristics of convection and flow patterns within the system. In cases with and without the circular object, higher values of *Pr* and *Ra* lead to a more pronounced cooling effect on the upper heated surface compared to the lower surface. Also, it enhances the overall thermal efficiency of the system by 112.05 % in comparison to the absence of a cylinder enclosure. These findings shed light on thermal control system advancements and contribute to field progress.

1. Introduction

Investigating fluid dynamics and heat transfer (HT) is essential for engineering systems' design and improvement [1]. This research explores entropy generation (E_{gen}) within differently shaped enclosed enclosures, exploring their significance across various domains such as industrial thermomechanical optimization, storage, and cooling systems [1]. By analyzing diverse enclosure shapes, this research thoroughly assesses flow and thermal properties under different thermophysical boundary conditions, encompassing temperature, heat flux, adiabatic, isothermal, and mixed parameters. These factors significantly impact flow behaviors, temperature variations, and E_{gen} within the enclosures. Hussein et al. [2] demonstrated that HT and temperature dispersion under an isothermal case significantly affect E_{gen} rates and distributions in enclosures with natural convection (NC). Cho et al. [3] investigated NC and *Egen* within a nanofluid (NF) filled U-shaped enclosure, exploring how varying thermal conditions impact HT and system performance.

Studying the intricacies of NC involves watchful observation of buoyancy-induced flow. Oliveski et al. [4] investigated this phenomenon through numerical analysis within a rectangular enclosure, while a similar observation was made by Yilbas et al. [5] for square enclosure. Chandra Roy et al. [6] conducted a thorough examination, identifying variables like magnetic field orientation, heating, porous boundaries, and nanoparticles density play critical roles in shaping flow and temperature patterns, thereby inducing significant transformations. Through numerical study, Momoniat et al. [7] revealed that the introduction of extended surfaces markedly altered temperature gradients, velocity patterns, and flux distributions within the square enclosure. Akhter et al. [8] explored HT via NC in a partially heated enclosure, noting the significant influence of buoyancy-induced flow on local E_{gen}, fluid dynamics, and temperature gradients. Kuyper et al. [9] explored the impact of laminar and turbulent flows on NC, establishing a strong correlation between *Ra* and Nusselt number (*Nu*).

Similarly, Kumar et al. [10] performed computational simulations within a rectangular enclosure, unveiling a clear correlation between average HT and buoyancy-induced flow, which escalates proportionally with *Ra*. Mobedi [11] conducted a computational study on NC within a square enclosure, elucidating heightened HT intensity between walls

* Corresponding author.
E-mail address: gsahamath@du.ac.bd (G. Saha).

https://doi.org/10.1016/j.ijft.2024.100785

Available online 2 August 2024

Nomenclature

Be	Bejan number
Be_l	Local Bejan number
Pr	Prandtl number
Ra	Rayleighnumber
Nu	Nusseltnumber
Nu_{avg}	AverageNusseltnumber
E_{avg}	Averageentropygeneration
E_{gen}	Entropygeneration
k	Thermalconductivity (W/m.K)
L	Length (m)
H	Heightofcavity (m)
S	Dimensionlessentropygeneration
T	Temperature (K)
T_f	Referencetemperature (K)
T_c	Coldtemperature (K)
T_h	Hottemperature (K)
u, v	Velocitycomponentsinxandydirections (m/s)
U, V	Dimensionlessvelocitycomponents
x, y	DimensionalCartesiancoordinates (m)
X, Y	Dimensionless Cartesian coordinates
S_{lhd}	Entropy generation due to temperature gradient
S_{lfd}	Entropy generation due to viscous dissipation
E_{total}	Totalentropygeneration

Greek Symbols

α	ThermalDiffusivity (m^2/s)
Ψ	Streamfunction
Ω	Vorticity
φ	Irreversibility Factor
ν	KinematicViscosity (m^2/s)
θ	DimensionlessTemperature
μ	Viscosity (Ns/m^{-2})
ρ	Density (kg/m^3)
g	Gravitational acceleration (ms^{-2})

Subscripts

avg	Average
c	Cold
f	Base Fluid
h	Hot
l	Local
t	Total

Abbreviation

NC	Natural convection
NF	Nanofluid
FC	Forced convection
HT	Heat transfer
ECOP	Ecological Coefficient Performance
FEM	Finite element method
WOC	Without cylinder
WC	With cylinder

with increasing *Ra* and improved conductivity ratios. Moreover, irregularities in enclosure shape significantly alter flow and HT behaviors, underscoring the importance of comprehending buoyancy-induced flow effects in such configurations for diverse applications like passive solar techniques and architectural exteriors [12].

Chaabane et al. [13] performed a computational exploration into the influence of an irregular enclosure shape on buoyancy-driven flow. Following this, Hatami et al. [14] conducted a thorough examination of natural convection HT in NF filled rectangular chamber featuring multiple fins. The results unveiled that increasing the fin height augmented the heated surface area, thereby elevating the average temperature through enhanced HT. Consequently, Yousaf et al. [15] explored natural convection HT within a square enclosure with sinusoidal roughness features. Their results demonstrated that the simultaneous arrangement of sinusoidal roughness on both hot and cold sides led to a noteworthy 28 % reduction in average HT. Sheremet et al. [16] conducted a computational analysis of E_{gen} within a corrugated enclosure. Their results elucidated that increasing *Ra* enhanced HT and modified the core convective flow while influencing recirculation patterns within the enclosure. Following this, Saha et al. [17] carried out a numerical investigation on NC flow of NF within a corrugated square enclosure. The study demonstrated that the presence of a corrugated wall substantially improved overall HT, thus enhancing thermal efficiency. Siavashi et al. [18] investigated NC within an enclosure featuring porous fins in a separate research effort. Their numerical results indicated that utilizing permeable fins with a substantial Darcy number (*Da*) enhanced HT. In contrast, the use of fins with a low *Da* could delay convection and decrease *Nu*. Recently, Ikram et al. [19] conducted an analysis of transient flow and HT in a divided, hexagon-shaped chamber filled with air under forced convection (FC) conditions, employing a dynamic modulator. Their findings revealed a notable enhancement in HT effectiveness compared to a standard enclosure domain. Furthermore, the research demonstrated that as the Reynolds number (*Re*) increased, so did the HT rate. In a related study, Ikram et al. [20] explored the unstable characteristics of conjugate HT within a hexagonal enclosure. Their results showcased an augmented HT efficiency in the enclosure by utilising a multi-blade dynamic modulator. In 2023, Saha et al. [21] introduced a comprehensive systematic literature survey on HT in enclosures. This analysis encompassed a broad spectrum of areas regarding enclosure's HT, including radiation, magnetic field effects, forced, mixed, and NC. It highlighted that the HT performance in enclosures is significantly influenced by various factors such as boundary conditions, heat sources, and fluid types. Moreover, applying visualization techniques such as streamline and isotherm plots has dramatically facilitated the analysis of flow patterns and temperature distribution [22]. These insights significantly enhance our understanding of the cavity's performance. Consequently, by scrutinizing this behavior, we can advance towards developing a more efficient cooling system and achieve superior temperature distribution across the entire system [23].

Novelty of the study

In this study, the use of decagonal enclosure provides new insights into the behavior of natural convection and heat transfer within this structure, particularly under varying thermal conditions. A notable innovation in this study is the incorporation of a heated cylinder within the decagonal enclosure. This cylinder simulates an actual electronic component, such as a microprocessor chip, generating heat that must be effectively dissipated to prevent overheating. This setup closely connected to real-world applications, thereby enhancing the practical relevance of the research. Moreover, the research focuses on developing a sophisticated cooling system designed to improve thermal management in electronic devices. Also, by integrating adiabatic inclined surfaces and cold vertical surfaces, the study aims to enhance the efficiency of heat dissipation, thereby improving the overall performance of electronic systems. In addition, the study extensively examines various boundary conditions, including the presence and absence of a heated cylinder, to assess their impact on heat transfer and entropy generation.

This thorough approach provides a detailed understanding of how different configurations influence thermal performance. Also, by analyzing entropy generation within the enclosure, the study sheds light on the thermodynamic efficiency of the cooling system. This focus on entropy provides a deeper understanding of the irreversibilities and energy losses within the system, which is crucial for designing more efficient thermal management solutions. At the end, the research introduces the concept of Ecological performance Coefficient (ECOP) to evaluate the ecological and energy efficiency of the cooling system.

2. Physical model

This study illustrates the decagonal enclosure depicted in Fig. 1, and the thermophysical properties of fluids are shown in Table 1. The inner cylinder has a radius of 0.2 L, while the decagon has a side length of L. To facilitate HT simulation in the physical model, the colder walls on the sides of the left (BC, CD) and right (GH, HI) are maintained at a constant temperature T_c. The cylinder, as well as horizontal walls (EF, AJ), are designated as hot (T_h). The remaining walls are treated as adiabatic.

3. Mathematical model

The fundamental equations that govern the scenario under analysis incorporate the principles of mass, momentum, and energy conservation within the fluid domain contained by a decagonal enclosure and the heat conduction equations for the heated wall. Our models use assumptions regarding Newtonian properties and incompressible flow, illustrating a continuous and smooth flow through their mathematical expressions. The examination takes into account two different working fluids: air and water. The governing equations are transformed into a dimensionless format by employing specific dimensionless variables, along with their respective boundary conditions, as detailed below:

$$X = \frac{x}{L},\ Y = \frac{x}{L},\ U = \frac{u}{\alpha L}, V = \frac{v}{\alpha L},\ \theta = \frac{(T_f - T_c)}{(T_h - T_c)} \tag{1}$$

Where α and L represent thermal diffusivity and length, respectively. Additionally, θ, T_f,T_c,*and*$T_h$represent dimensionless temperature, reference temperature, cold temperature and hot temperature, respectively.

To visualize the stream function, the continuity equation is converted into the stream function equation using Eq. (2). Similarly, the vorticity equation is derived using the vorticity stream function method, facilitating the elimination of the pressure term from the momentum equation. The dimensionless stream function and vorticity are presented as follows [23,24]:

$$U = \frac{\partial \Psi}{\partial Y},\ V = \frac{\partial \Psi}{\partial X}\ and\ \frac{\partial V}{\partial X} - \frac{\partial U}{\partial Y} = \Omega \tag{2}$$

Table 1
Thermophysical properties of Air and water [22].

Property	Air	Water
Density ($kg.m^{-3}$)	1.204	997.1
Specific heat ($J.kg^{-1}K^{-1}$)	1006.1	4179
Thermal conductivity (W. m^{-1} K^{-1})	0.0256	0.613
Expansion coefficient × $10^{-5}(K^{-1})$	343	21

Where the variable Ψ and Ω stand for stream function and vorticity, respectively.

Hence, the two-dimensional governing equations are depicted in non-dimensional format as follows [24]:

$$\frac{\partial^2 \Psi}{\partial X^2} + \frac{\partial^2 \Psi}{\partial Y^2} = -\Omega \tag{3a}$$

$$U\frac{\partial \Omega}{\partial X} + V\frac{\partial \Omega}{\partial Y} = Pr\left(\frac{\partial^2 \Omega}{\partial X^2} + \frac{\partial^2 \Omega}{\partial Y^2}\right) \tag{3b}$$

$$U\frac{\partial \Omega}{\partial X} + V\frac{\partial \Omega}{\partial Y} = Pr\left(\frac{\partial^2 \Omega}{\partial X^2} + \frac{\partial^2 \Omega}{\partial Y^2}\right) + RaPr\frac{\partial \theta}{\partial X} \tag{3c}$$

$$\left(U\frac{\partial \theta}{\partial X} + V\frac{\partial \theta}{\partial Y}\right) = \left(\frac{\partial^2 \theta}{\partial X^2} + \frac{\partial^2 \theta}{\partial Y^2}\right) \tag{3d}$$

Where *U, V, θ, X, Y* represent non-dimensional variables, and the non-dimensional parameters found in the governing equations encompass *Ra* and *Pr*, which are presented as [23]:

$$Ra = \frac{g\beta(T_h - T_c)L^3}{\vartheta\alpha},\ Pr = \frac{\mu}{\rho\alpha} \tag{3e}$$

Boundary conditions:
For Adiabatic Walls:

$$U = V = 0,\ \Psi = \frac{\partial \theta}{\partial n} = 0$$

for AB : $L_1 = 1.8L,\ A \le X \le -\cos\pi L_1$ and $A \le Y \le -\cos\pi L_1$

for DE : $L_4 = 1.2L,\ -\cos\pi L_3 \le X \le E$ and $-\sin\pi L_3 \le Y \le -\cos\pi L_4$

for FG : $L_5 = 0.8L,\ F \le X \le -\cos\pi L_5$ and $F \le Y \le \sin\pi L_5$

for IJ : $L_8 = 0.2L,\ -\cos\pi L_7 \le X \le -\cos\pi L_8$ and $\sin\pi L_7 \le Y \le \sin\pi L_8$

For Cold Walls:

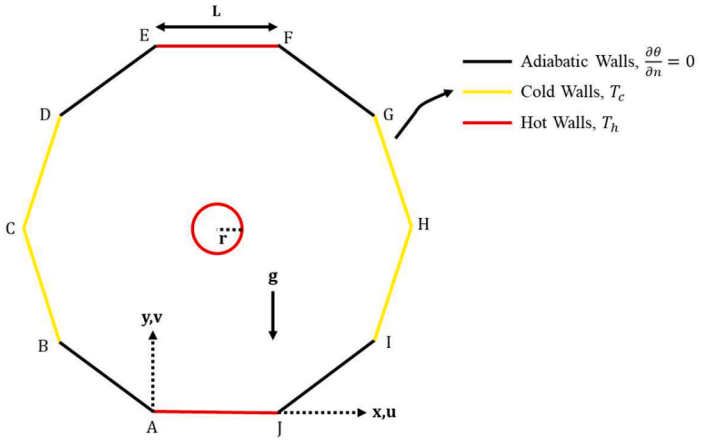

Fig. 1. A schematic view of the physical model.

$$U = V = \Psi = 0,\ T = T_c$$

for BC : $L_2 = 1.6\text{L},\ -\cos\pi L_1 \le X \le -\cos\pi L_2$ and $-\sin\pi L_1 \le Y \le -\sin\pi L_2$

for CD : $L_3 = 1.4\text{L},\ -\cos\pi L_2 \le X \le -\cos\pi L_3$ and $-\sin\pi L_2 \le Y \le -\sin\pi L_3$

for GH : $L_6 = 0.6\text{L},\ -\cos\pi L_5 \le X \le -\cos\pi L_6$ and $\sin\pi L_5 \le Y \le \sin\pi L_6$

for HI : $L_7 = 0.4\text{L},\ -\cos\pi L_6 \le X \le -\cos\pi L_7$ and $\sin\pi L_6 \le Y \le \sin\pi L_7$

For Heated Walls:

$$U = V = \Psi = 0,\ T = T_h$$

for EF : $Y = 0$ and $E \le X \le F$

for JA : $Y = 0$ and $J \le X \le A$

for cylinder : $X = \frac{L}{2}$ and $Y = \frac{L}{0.65}$

Entropy Generation:

The system's thermal efficiency is assessed through an E_{gen} analysis. Subsequently, the enclosure's thermal performance is assessed, relying on the results of this investigation. The total entropy generation (E_{total}) is represented in the non-dimensional format as follows [25]:

$$E_{total} = S_{lhd} + S_{lfd} \tag{4a}$$

$$S_{lhd} = \left[\left(\frac{\partial\theta}{\partial x}\right)^2 + \left(\frac{\partial\theta}{\partial y}\right)^2\right] \tag{4b}$$

$$S_{lfd} = \varphi\left[2\left(\frac{\partial u}{\partial x}\right)^2 + 2\left(\frac{\partial v}{\partial y}\right)^2 + \left(\frac{\partial u}{\partial y} + \frac{\partial v}{\partial x}\right)^2\right] \tag{4c}$$

Here, the irreversibility factor, represented by φ in this case, is 10^{-4} [19].

The local Bejan number (Be_l), average entropy generation (E_{avg}), average Bejan number (Be_{avg}), and the average Nusselt number (Nu_{avg}) are presented as follows [18,24,26,27]:

$$Be_l = \frac{S_{lhd}}{E_{total}} \tag{5a}$$

$$E_{avg} = \frac{\int\int E_{total}\ \mathrm{dx\ dy}}{\int\int\ \mathrm{dx\ dy}} \tag{5b}$$

$$Be_{avg} = \frac{\int_A\int_A Be_l\ \mathrm{dx\ dy}}{\int_A\int_A\ \mathrm{dx\ dy}} \tag{5c}$$

$$Nu_{avg} = \left[\int \frac{\partial\theta}{\partial y}\Big|_{bottom\ wall}\ dx + \int \frac{\partial\theta}{\partial y}\Big|_{top\ wall}\ dx\right] \tag{5d}$$

Ecological performance Coefficient (ECOP):

Assessing an enclosed system's performance and ecological sustainability is paramount, and the Ecological Performance Coefficient plays a crucial role in this evaluation. It offers valuable insights into the efficiency of resource utilization in achieving desired outcomes, all while considering environmental factors. It is defined as follows [28]:

$$ECOP = \frac{Nu_{avg}}{E_{avg}} \tag{6}$$

4. Methodology and validation

The finite element method (FEM) implemented in the COMSOL Multiphysics application has successfully solved the governing equations (3a-d) and their corresponding boundary conditions [17,19,27]. This is achieved by transforming the governing partial differential equations (PDEs) into integral equations using the Galerkin weighted residual technique. The FEM, employing second-order approximation, is chosen for its ability to ensure rapid convergence and visualize results effectively.

A graphical representation of the chosen research methodology is illustrated in Fig. 2, with further elaboration provided in subsequent sections.

Linear discretization techniques are specifically applied to model HT within the fluid domain. Non-uniform triangular mesh elements are employed to discretize various flow variables across the computational domain. Error criteria are assessed using a relative tolerance of 10^{-6}. In order to guarantee accuracy and reliability, a grid independence assessment is carried out by altering grid sizes while maintaining

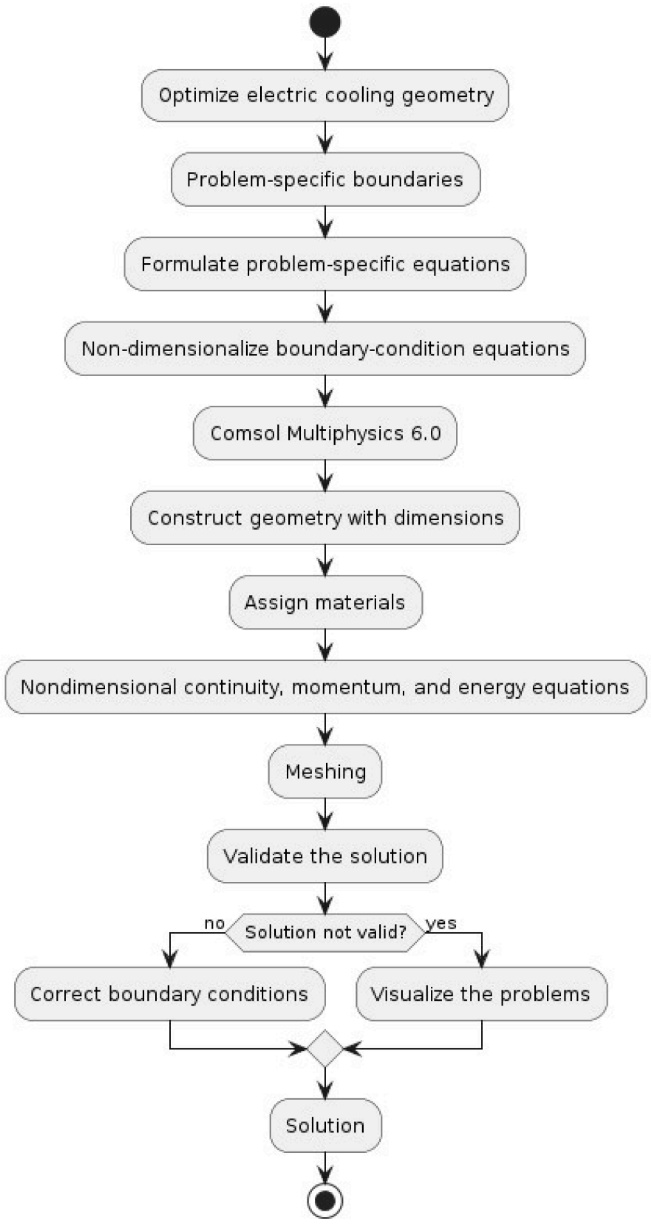

Fig. 2. Methodology flowchart.

constant parameters. This evaluation aims to determine the most suitable grid size for the investigation. Employing a triangular mesh, grid sizes spanning from 10,170 to 49,052 elements are tested, and the results are displayed in Table 2. After the comparison, a grid size of 45,532 is identified as the optimal choice for the investigation.

To ensure the reliability of our computational methodology and validate the obtained results, we meticulously compared the streamlines and isotherms for incompressible flow at Ra = 10^5 and 10^6 within the octagonal enclosure. This comparison is illustrated in Fig. 3, and a comprehensive analysis is presented in Table 3, indicating an error of less than 1 %. The results qualitatively align with previous findings documented by Saboj et al. [27]. It is apparent that our results demonstrate a high degree of consistency, thus confirming the precision of our numerical simulations.

Moreover, Fig. 4 compares our present isothermal contour findings with those from an experimental investigation conducted by Corvaro et al. [29]. This comparison centers on a rectangular enclosure containing air and subjected to heating from a small, localized source on the bottom wall. Remarkably, the figure highlights a good agreement between the results. Furthermore, validation of E_{gen} is performed through another comparison, as shown in Fig. 5. This visual representation highlights the substantial agreement between our findings and the earlier work by Ilis et al. [23], thus augmenting the accuracy of the overall assessment of E_{gen} throughout the system.

5. Results and discussion

This computational study investigates HT and fluid dynamics phenomena in a decagonal enclosure. It considers scenarios with and without the inclusion of a heated cylinder to assess their respective influences on the observed phenomena, considering $10^3 \leq Ra \leq 10^6$ and $0.71 \leq Pr \leq 7$. This research uses streamlines, isothermal contours, E_{gen}, and *Be* as analytical tools to investigate flow phenomena and HT characteristics.

5.1. Decagonal enclosure without hot cylinder

This section explores the graphical representations and solutions generated from our mathematical model. We examine and interpret the outcomes of the decagonal enclosure both in the absence and presence of a hot cylinder across various *Ra* ($Ra = 10^3$ - 10^6). Fig. 6 illustrates isotherms, streamlines, E_{total}, and *Be* contours for different *Ra* values. Each contour is subject to alterations with changing *Ra*, reflecting the influence of thermal buoyancy forces on temperature and stream functions. Thermal buoyancy forces exhibit relatively subdued effects at lower *Ra* = 10^3, leading to less pronounced isotherm and streamline contours within the enclosure. Nonetheless, the symmetry of the isotherm contours may be impacted by diverse factors, including the enclosure's geometry and the distribution of convection effects along its walls. In the scenario of a decagonal enclosure, where varying convection effects are apparent on its walls, the symmetry of the isotherm contours is disrupted, resulting in temperature distribution asymmetry. Consequently, substantial regional temperature variations may arise within the enclosure. For example, isotherms adjacent to the cold walls may display parallel contours, whereas those near the hot walls may exhibit closely spaced contours. Moreover, water's higher density and thermal conductivity, in contrast to air, facilitate more efficient heat transmission. Water raises larger and more resilient convection cells compared to air, leading to smoother and more orderly streamline patterns, even at identical *Ra*. At $Ra = 10^3$, the streamline contours fill the entire enclosure symmetrically. Significantly, with the increase of *Ra*, there is a notable augmentation in flow intensity, which is evident in the streamlines. At $Ra = 10^4$, the streamline contours expand, while at $Ra = 10^5$, these curves evolve into intricately twisted formations departing from parallel alignment. Higher *Ra* values, such as $Ra = 10^5$ and 10^6, introduce intensified complexity and a touch of chaos to the streamline dynamics. As *Ra* increases, the convection circulation gains momentum, causing the isotherms near the cooler walls to converge. Within the $Ra = 10^4$ to 10^6 range, the isotherm contours become more tightly spaced near the hot surface, forming twisted flattened curves near the cold surface. Concerning E_{gen}, elevating *Ra* considerably increases total E_{gen} contours adjacent to the cold walls on both sides. Likewise, at $Ra = 10^6$, vortices become apparent near the cold wall, mainly when viscous dissipation substantially affects the overall geometry. This phenomenon results in increased HT rates near the lower hot boundary. Moreover, heightened values of local Be_l are noted near the wall boundaries, indicating more efficient HT in those regions.

Table 2
Mesh Independence Test for Nu_{avg} with (*Pr, Ra*) = (7.0, 10^6).

Number of Elements	Nu_{avg}	|*Error*|%
10,170	13.767	–
13,978	13.793	0.189
16,352	13.796	0.022
19,098	13.798	0.015
23,440	13.802	0.029
27,994	13.825	0.167
37,038	13.856	0.224
43,506	13.881	0.180
45,532	**13.886**	0.036
49,052	13.888	0.0144

5.2. Decagonal enclosure with hot cylinder

Fig. 7 shows the contours of various parameters such as isotherms, streamlines, E_{total}, and *Be* within a decagonal enclosure consisting of a heated cylinder, showcasing the dynamic effects of different *Ra* values. Notably, each contour undergoes visible shifts as *Ra* change, reflecting the substantial impact of these factors on the flow behavior within the enclosure. At $Ra = 10^3$, the isotherm contours display a distinct pattern with twisted parallel curves near the cold surfaces and flatter twisted curves adjacent to the hot surfaces. With an increase in *Ra* from 10^4 to 10^6, thermal buoyancy forces intensify significantly. Consequently, the isotherm contours transform into tightly twisted parallel curves near the hot surfaces, maintaining symmetry while appearing as closely spaced parallel curves near the cold surfaces. This shift signifies the increasing dominance of thermal buoyancy forces, marking a transition towards convective mode in thermal and mass transport regimes.

At $Ra = 10^3$, symmetrical rotating vortices indicate a coherent flow pattern regarding streamline contours. However, as *Ra* rises to 10^6, streamline contours become more pronounced and expansive, evolving into a complex symmetrical nature with hints of chaos, indicating higher convection within the flow. Moreover, at higher *Ra* values, convective processes have a more pronounced effect on fluid motion and E_{gen}, resulting in noticeable differences in E_{gen} between different temperature domains. It is seen that increased *Ra* substantially raises contours near cold walls and the cylinder while decreasing them near the top heated wall, suggesting greater HT efficiency at the top wall. As *Ra* increases, more vortices emerge near cold and cylinder walls due to dominant viscous dissipation, leading to increase HT rates throughout the system. The Bejan number follows a similar trend as observed without the cylinder but with values clustered near walls, resulting in an overall decrease in *Be* and enhanced system efficiency.

5.3. Variations of Prandtl numbers

Fig. 8 presents the contours of isotherms and streamlines across various *Pr* at Ra = 10^6. When Pr is low (= 0.71), the streamlines show a symmetrical pattern with rotating twisted vortices inside the enclosure without a hot cylinder. With increasing *Pr*, the streamlines become smoother and parallel, transitioning to symmetrical spreading within the enclosure at *Pr* = 7. However, in the presence of a hot cylinder,

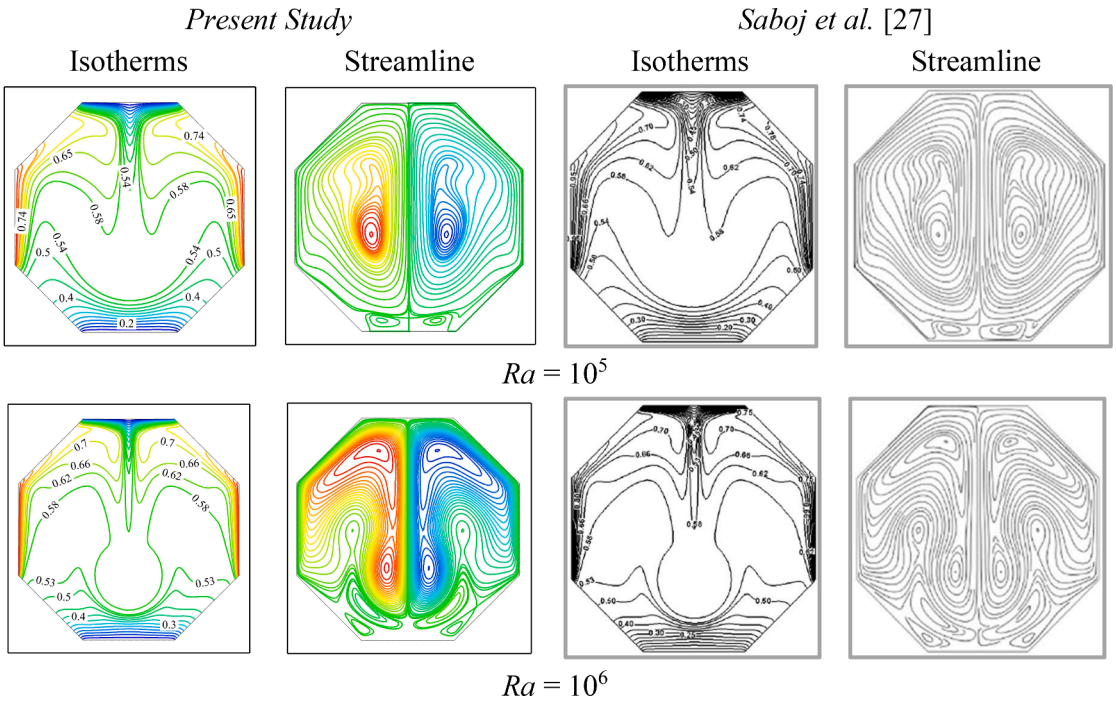

Fig. 3. Comparative analysis of isotherm and streamline profiles between the present study and Saboj et al. [27] results for (i) $Ra = 10^5$ and (ii) $Ra = 10^6$ at $Pr = 0.71$.

Table 3
Comparison of Nu_{avg} results for natural convection of Octagonal Cavity.

Ra	Nu_{avg}		*Error (%)*
	Saboj et al. [27]	*Present*	
10^3	2.42	2.4247	0.194 %
10^4	4.20	4.2032	0.0761 %
10^5	6.81	6.8270	0.24963 %
10^6	11.22	11.262	0.3743 %

higher *Pr* led to progressively intricate symmetrical patterns in the streamlines, marked by chaotic behavior, which intensifies with higher *Pr*. At $Pr = 7$, the streamlines show a complex, chaotic pattern symmetrically distributed within the enclosure.

Meanwhile, the isotherm contours demonstrate distinctive curves corresponding to different *Pr*, reflecting variations in HT and fluid behavior within the enclosure. As *Pr* increases, the walls of the enclosure exhibit diverse convection effects while maintaining a constant higher $Ra = 10^6$. Higher *Pr* results in parallel curves along the hot walls and twisted curves along the cold walls within the enclosure in the absence of a hot cylinder. Conversely, decreasing *Pr* led to chaotic isotherm contours within the hot cylinder enclosure. Specifically, at *Pr* of 2.8 and 4.9, the isotherm contours display twisted curves within the enclosure. However, at $Pr = 0.71$, the isotherm contours show a complex symmetrical curve near the enclosure's hot and cold surfaces, reflecting intricate convection patterns resulting from fluid dynamics interactions within the enclosure.

5.4. Quantitative analysis

Table 4 presents a results of flow characteristics of air and water. It is apparent that as *Ra* increases, Nu_{avg} rises in both scenarios, with and without the presence of a hot cylinder. Notably, in the case of water, Nu_{avg} is significantly more pronounced in both scenarios. This disparity is attributed to water's superior ability to facilitate smoother and more uniform HT throughout the system compared to air. Moreover, it is apparent that the average E_{gen} increases with higher *Ra* values. The heat source surfaces display notable temperature and concentration gradients, leading to localized irreversible characteristics due to the thermal transport effect. Remarkably, the irreversible conditions induced by fluid flow friction effects (viscous dissipation) outweigh those arising from the thermal transfer effect, as evidenced by the local E_{total} and local *Be* distributions and their respective values. In both cases, Nu_{avg} and E_{avg}

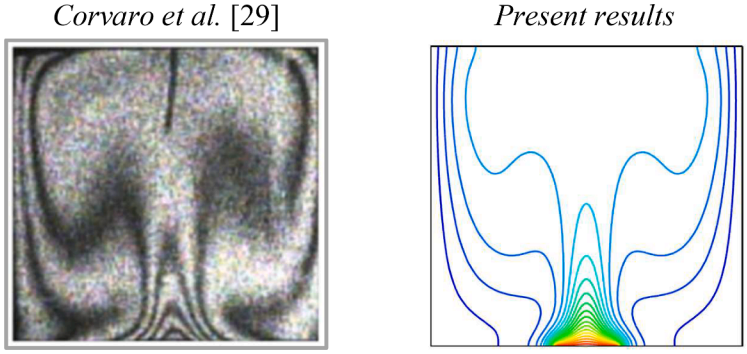

Fig. 4. Comparative analysis of isothermal contours between present results and experimental results of Corvaro et al. [29] for $Ra = 2.02 \times 10^5$.

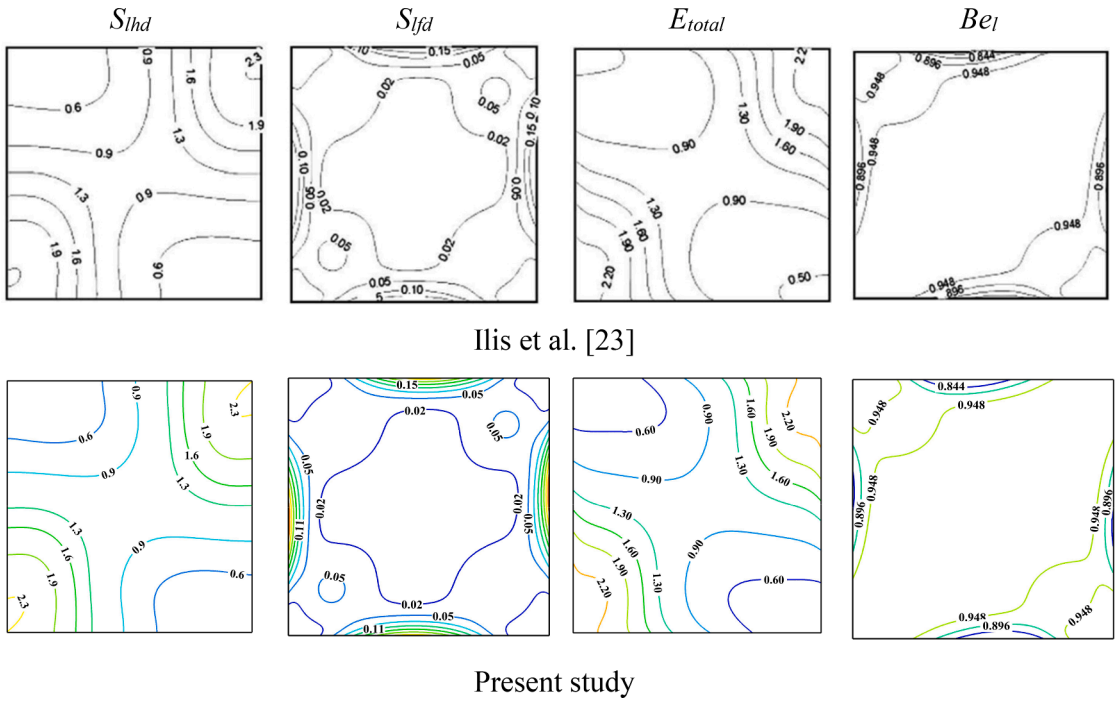

Fig. 5. Comparative analysis of S_{lhd}, S_{lfd}, E_{total}, and Be_l at $Ra = 10^3$ and aspect ratio = 1 between Ilis et al. [23] and present study.

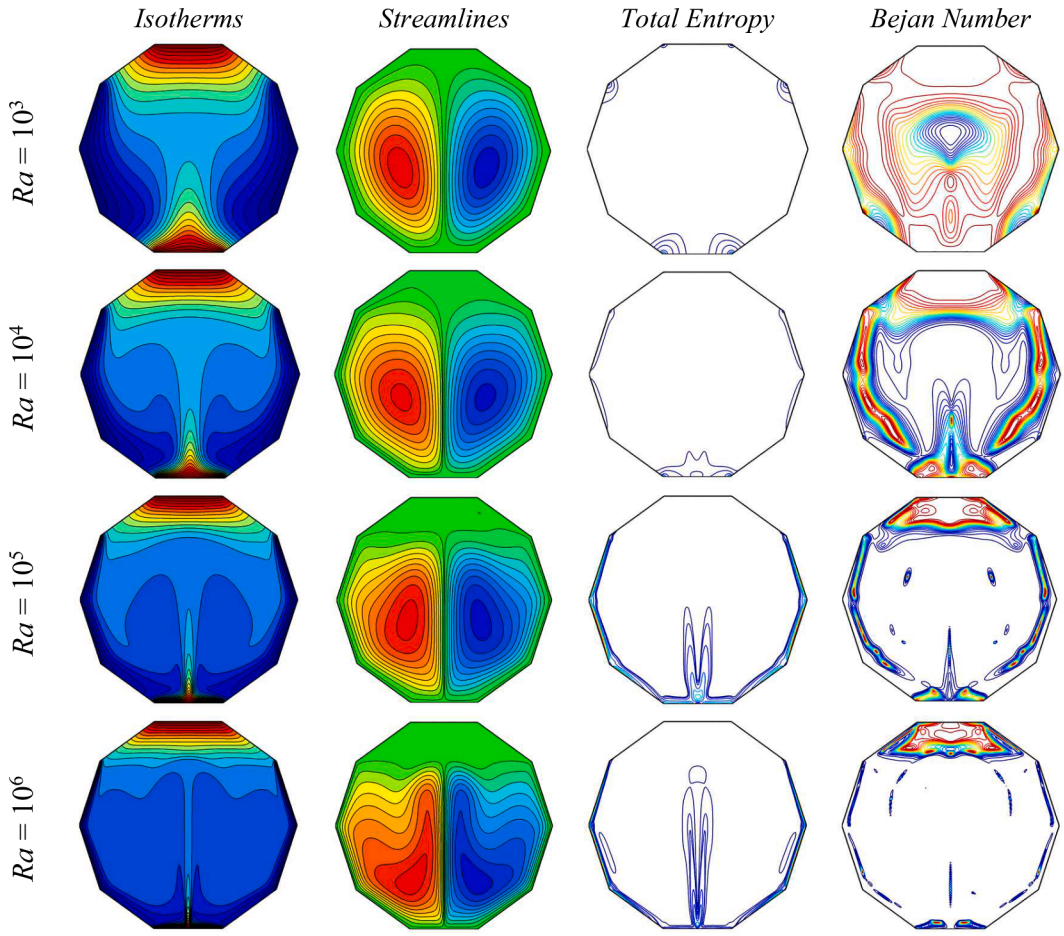

Fig. 6. Variation of Isotherms, Streamlines, Total Entropy, and Bejan Number for different *Ra* values and Pr = 7.0.

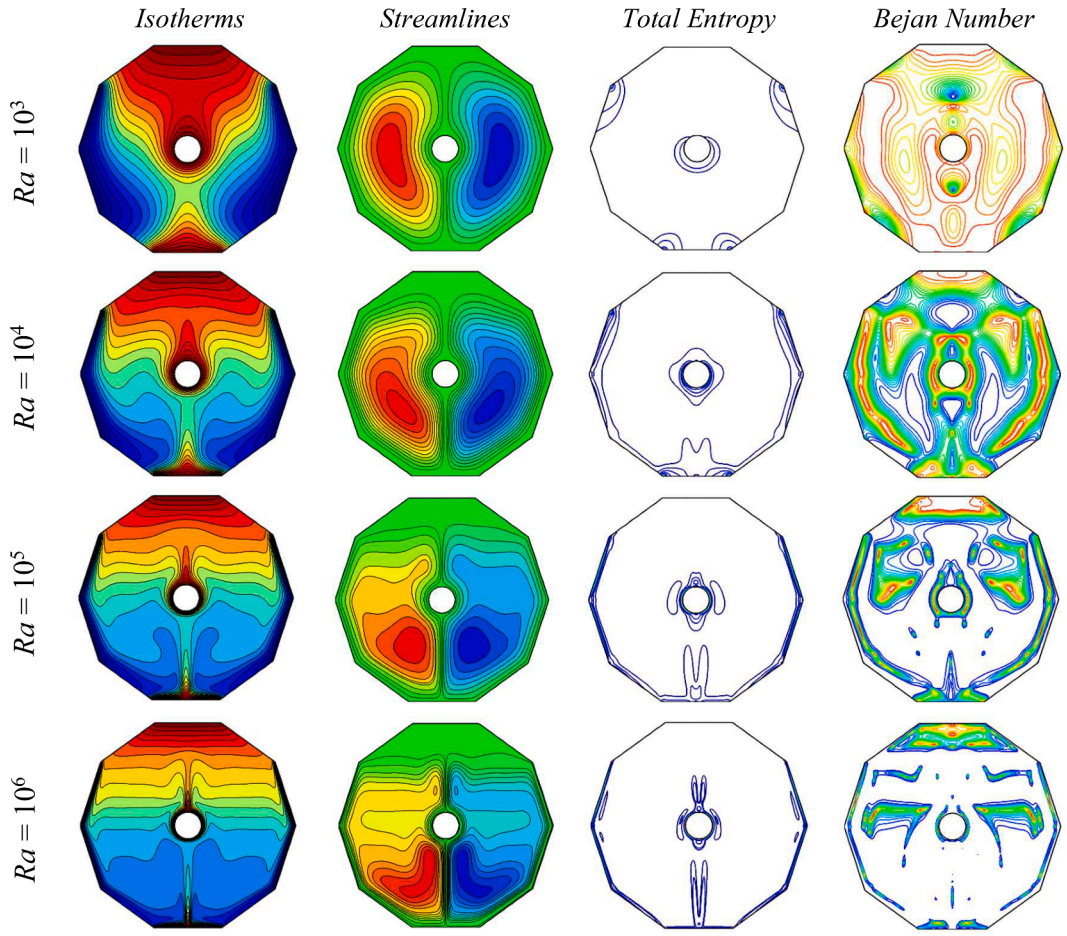

Fig. 7. Variation of Isotherms, Streamlines, E_{total}, and *Be* for different *Ra* values and $Pr = 7.0$.

exhibit rapid enhancements with increasing *Ra* in both scenarios, with and without a hot cylinder inside the enclosure.

Fig. 9 illustrates the average Nusselt number, total entropy generation, and Bejan number at different Rayleigh numbers for both cases: WOC and WC. It is evident that both the Nusselt number and total entropy generation increase steadily with increasing Rayleigh values, indicating improved heat distribution performance overall. In the case of WOC, the average Nusselt number increased by 10.5221 % when changing the *Pr* value from 0.71 to 7. This increase is attributed to the dominant role of convection as the Prandtl number increases, thereby enhancing overall thermal performance. Similarly, for WC, overall performance increased by 2.47354 % with the change in *Pr* values. It is notable that at a Rayleigh value of 10^5, total entropy generation increases. At these values, the flow region transitions from conductive dominance to convective dominance, particularly evident in the case of WOC at $Pr = 7$. Conversely, an inverse trend is observed in the Bejan number; as Rayleigh values increase, the overall Bejan number decreases, indicating a more balanced fluid flow and heat transfer, particularly in the case of WC.

5.5. Ecological coefficient performance

Fig. 10 illustrates the impact of varying Ra on the Ecological Coefficient Performance (ECOP) in scenarios with and without a heated cylinder. The graph illustrates that increasing *Ra* leads to a notable decline in ECOP, resulting in diminished energy efficiency and heightened environmental impact. This trend persists consistently, indicating a continuous decrease in ECOP values with rising *Ra*, thereby lowering energy efficiency and escalating ecological impact throughout the system. Similar observations can be made with increasing *Pr* values. Remarkably, cases involving a cylinder exhibit superior energy efficiency and reduced environmental impact compared to those without a cylinder.

6. Conclusions

The present study presents a computational examination of NC and E_{gen} within a decagonal enclosure. This enclosure comprises two heated walls at the top and bottom, along with four cold walls on the sides. Additionally, it includes four adiabatic walls at the corners. The main findings are summarized below:

- The Prandtl and Rayleigh numbers serve as critical determinants of a system's flow behavior and convection characteristics.
- In scenarios with and without a cylinder, higher values of the Prandtl and Rayleigh numbers lead to a more significant cooling effect on the top heated wall than the bottom wall.
- The incorporation of a heated cylinder into the geometry fosters a homogeneous dispersion of heat transfer throughout the system, thereby yielding a more uniform and consistent cooling effect across the entirety of the domain.
- At elevated Rayleigh numbers, the inclusion of a heated cylinder exacerbates the chaotic dynamics, thereby amplifying turbulence, convective processes, and overall entropy generation. Consequently, this augmentation enhances heat transfer across the system, thereby contributing to a more efficient thermal energy management system.

Hence, introducing a conductive cylinder into a cavity generally

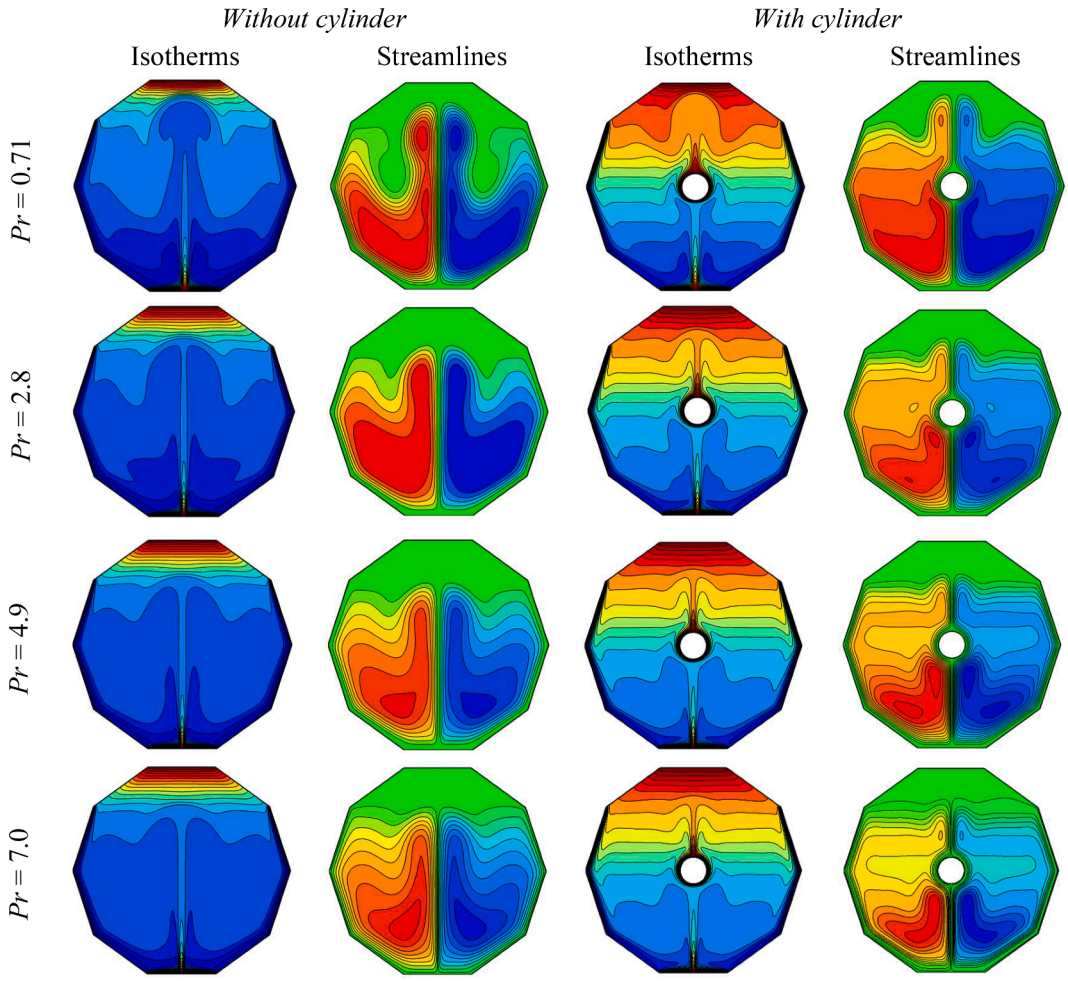

Fig. 8. Variation of streamlines and isotherms for different *Pr* with $Ra = 10^6$.

Table 4
Results of flow characteristics of air and water.

Without Cylinder				*With Cylinder*			
Air							
Ra	Nu_{avg}	E_{avg}	*Be*	*Ra*	Nu_{avg}	E_{avg}	*Be*
10^3	2.9419	3.3351	0.79929	10^3	4.903	5.4953	0.8606
10^4	5.0529	10.087	0.37929	10^4	8.928	16.902	0.48208
10^5	7.9673	88.154	0.12061	10^5	15.294	146.23	0.2087
10^6	12.564	1553.6	0.03992	10^6	26.642	2301.6	0.13002
Water							
Ra	Nu_{avg}	E_{avg}	*Be*	*Ra*	Nu_{avg}	E_{avg}	*Be*
10^3	3.0308	3.4597	0.78958	10^3	4.9574	5.57	0.8462
10^4	5.4067	12.37	0.33755	10^4	9.2903	18.581	0.42253
10^5	8.7112	127.93	0.12516	10^5	16.032	172.8	0.17255
10^6	13.886	2080.8	0.074762	10^6	27.301	2671.4	0.076257

enhances the overall thermal performance of the system, resulting in a significant improvement of 112.05 % for air and 96.61 % for water. This enhancement can lead to better performance of microprocessors, as the cooling rate is maximized, thereby helping to maintain optimal operating temperatures and potentially increasing efficiency and reliability.

7. Limitations and future studies

The current research explores specific aspects of HT and E_{gen} within distinct boundary conditions. Although this study focuses primarily on NC, practical situations frequently incorporate additional variables, such as forced convection, that influence HT patterns. Moreover, while non-dimensional analysis proves adequate for this examination, dimensional analysis is indispensable for real-world scenarios. Furthermore, the approach utilized relies on numerical analysis.

In order to enhance our comprehension of HT and E_{gen} in an enclosure, prospective research initiatives should strive to integrate nanofluids, examine changes in cylinder geometries, incorporate discrete heating, and scrutinize further phenomena including forced and mixed convection. These undertakings would not only expand our understanding but also provide crucial perspectives on optimizing thermal control systems and improving effectiveness in diverse fields of application.

Funding

This research received no external funding.

CRediT authorship contribution statement

Jahidul Islam Jihan: Writing – review & editing, Writing – original draft, Visualization, Validation, Software, Methodology, Investigation, Formal analysis. **Bijan Krishna Saha:** Writing – review & editing, Writing – original draft, Visualization, Validation, Software. **Preetom Nag:** Writing – review & editing. **Nur Jahangir Moon:** Writing – review & editing, Writing – original draft, Investigation. **Goutam Saha:** Writing – review & editing, Supervision, Investigation, Formal analysis, Conceptualization. **Suvash C. Saha:** Writing – review & editing,

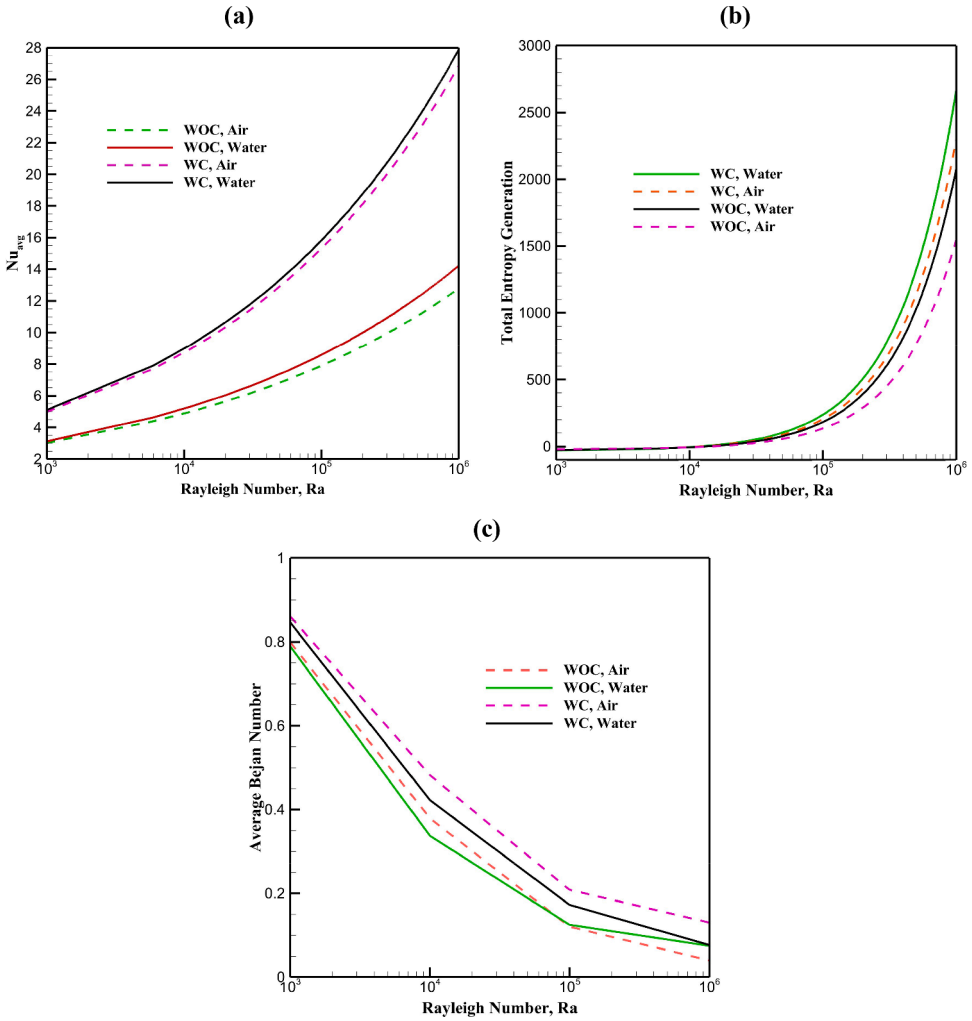

Fig. 9. a) Average Nusselt number; b) Total entropy generation; c) Bejan number with Ra in both the with and without cylinder cases at (Pr = 0.71 and 7.0).

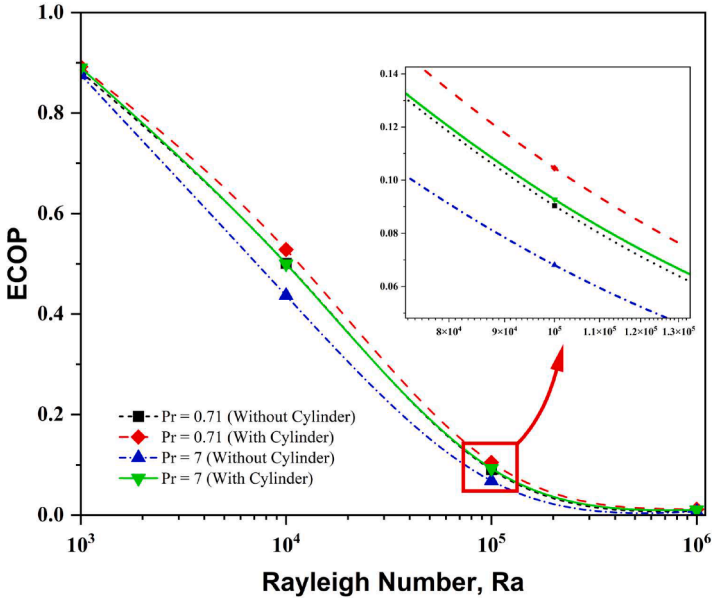

Fig. 10. Analysis of Ecological Coefficient Performance with and without Cylinder.

Supervision.

Declaration of competing interest

The authors declare that they have no known competing financial interests or personal relationships that could have appeared to influence the work reported in this paper.

Data availability

No data was used for the research described in the article.

References

[1] S. Saha, T. Sultana, G. Saha, M.M. Rahman, Effects of discrete isoflux heat source size and angle of inclination on natural convection heat transfer flow inside a sinusoidal corrugated enclosure, Int. Commun. Heat Mass Transfer 35 (10) (2008) 1288–1296, https://doi.org/10.1016/j.icheatmasstransfer.2008.08.005.

[2] A.K. Hussein, K. Lioua, R. Chand, S. Sivasankaran, R. Nikbakhti, D. Li, B.M. Naceur, B.A. Habib, Three-dimensional unsteady natural convection and entropy generation in an inclined cubical trapezoidal cavity with an isothermal bottom wall, Alexandria Eng. J. 55 (2) (2016) 741–755, https://doi.org/10.1016/j.aej.2016.01.004.

[3] C.C. Cho, H.T. Yau, C.H. Chiu, K.C. Chiu, Numerical investigation into natural convection and entropy generation in a nanofluid-filled U-shaped cavity, Entropy 17 (9) (2015) 5980–5994, https://doi.org/10.3390/e17095980 (Basel, Switzerland).

[4] R.D.C. Oliveski, M.H. Macagnan, J.B. Copetti, Entropy generation and natural convection in rectangular cavities, Appl. Therm. Eng. 29 (8) (2009) 1417–1425, https://doi.org/10.1016/j.applthermaleng.2008.07.012.

[5] B.S. Yilbas, S.Z. Shuja, S.A. Gbadebo, H.I.A. Al-Hamayel, K. Boran, Natural convection and entropy generation in a square cavity, Int. J. Energy Res. 22 (14) (1998) 1275–1290, https://doi.org/10.1002/(SICI)1099-114X(199811)22:14<1275::AID−ER453>3.0.CO;2-B.

[6] N. Chandra Roy, S. Monira, R. Subba Reddy Gorla, Buoyancy-driven flow of magnetohydrodynamic hybrid nanofluids in an open cavity with permeable horizontal walls. Proceedings of the Institution of Mechanical Engineers. Part N, J. Nanomaterials, Nanoengineering Nanosystems (2023), https://doi.org/10.1177/23977914231151481, 239779142311514.

[7] E. Momoniat, C. Harley, R.S. Herbst, Effects of extended surfaces on heat transfer in buoyancy-driven flow in a square cavity, Results. Eng. 18 (2023) 101190, https://doi.org/10.1016/j.rineng.2023.101190.

[8] R. Akhter, M. Mokaddes Ali, M.A. Alim, Entropy generation due to hydromagnetic buoyancy-driven hybrid-nanofluid flow in partially heated porous cavity containing heat conductive obstacle, Alexandria Eng. J. 62 (2023) 17–45, https://doi.org/10.1016/j.aej.2022.07.005.

[9 R.A. Kuyper, Th.H. Van Der Meer, C.J. Hoogendoorn, R.A.W.M. Henkes, Numerical study of laminar and turbulent natural convection in an inclined square cavity, Int. J. Heat. Mass Transf. 36 (11) (1993) 2899–2911, https://doi.org/10.1016/0017-9310(93)90109-J.

[10] A. Kumar, M.K. Sinha, Buoyancy driven flow through a square enclosure, Mater. Today - Proceedings 56 (2022) 2780–2784, https://doi.org/10.1016/j.matpr.2021.10.091.

[11] M. Mobedi, Conjugate natural convection in a square cavity with finite thickness horizontal walls, Int. Commun. Heat Mass Transfer 35 (4) (2008) 503–513, https://doi.org/10.1016/j.icheatmasstransfer.2007.09.004.

[12] A.D.A. Rejeesh, S. Udhayakumar, T.V.S. Sekhar, R. Sivakumar, Mixed Convection and Heat Transfer Studies in Non-Uniformly Heated Buoyancy Driven Cavity Flow, Open J. Fluid Dyn. 7 (2) (2017) 231–262, https://doi.org/10.4236/ojfd.2017.72016 (Irvine, CA).

[13] R. Chaabane, L. Kolsi, A. Jemni, A D'Orazio, Buoyancy driven flow characteristics inside a cavity equiped with diamond elliptic array, Int. J. Nonlinear Sci. Numer. Simul. 24 (6) (2023) 2163–2177, https://doi.org/10.1515/ijnsns-2021-0073.

[14] M. Hatami, Numerical study of nanofluids natural convection in a rectangular cavity including heated fins, J. Mol. Liq. 233 (2017) 1–8, https://doi.org/10.1016/j.molliq.2017.02.112.

[15] M. Yousaf, S. Usman, Natural convection heat transfer in a square cavity with sinusoidal roughness elements, Int. J. Heat. Mass Transf. 90 (2015) 180–190, https://doi.org/10.1016/j.ijheatmasstransfer.2015.06.049.

[16] M. Sheremet, I. Pop, H.F. Öztop, N. Abu-Hamdeh, Natural convection of nanofluid inside a wavy cavity with a non-uniform heating: entropy generation analysis, Int. J. Numer. Methods Heat. Fluid. Flow. 27 (4) (2017) 958–980, https://doi.org/10.1108/HFF-02-2016-0063.

[17] T. Saha, T. Islam, S. Yeasmin, N. Parveen, Thermal influence of heated fin on MHD natural convection flow of nanofluids inside a wavy square cavity, Int. J. Thermofluids 18 (2023) 100338, https://doi.org/10.1016/j.ijft.2023.100338.

[18] M. Siavashi, R. Yousofvand, S. Rezanejad, Nanofluid and porous fins effect on natural convection and entropy generation of flow inside a cavity, Adv. Powder Technol.: Int. J. Soc. Powder Technol. 29 (1) (2018) 142–156, https://doi.org/10.1016/j.apt.2017.10.021. Japan.

[19] M.M. Ikram, G. Saha, S.C. Saha, Conjugate forced convection transient flow and heat transfer analysis in a hexagonal, partitioned, air filled cavity with dynamic modulator, Int. J. Heat. Mass Transf. 167 (2021) 120786, https://doi.org/10.1016/j.ijheatmasstransfer.2020.120786.

[20] M.M. Ikram, G. Saha, S.C. Saha, Unsteady conjugate heat transfer characteristics in hexagonal cavity equipped with a multi-blade dynamic modulator, Int. J. Heat. Mass Transf. 200 (2023) 123527, https://doi.org/10.1016/j.ijheatmasstransfer.2022.123527.

[21] G. Saha, A.A.Y. Al-Waaly, M.C. Paul, S.C. Saha, Heat Transfer in Cavities: configurative Systematic Review, Energies 16 (5) (2023) 2338, https://doi.org/10.3390/en16052338 (Basel).

[22] F. Mebarek-Oudina, R. Fares, A. Aissa, R.W. Lewis, N. H. Abu-Hamdeh, Entropy and convection effect on magnetized hybrid nano-liquid flow inside a trapezoidal cavity with zigzagged wall, Int. Commun. Heat Mass Transfer 125 (2021) 105279, https://doi.org/10.1016/j.icheatmasstransfer.2021.105279.

[23] G.G. Ilis, M. Mobedi, B. Sunden, Effect of aspect ratio on entropy generation in a rectangular cavity with differentially heated vertical walls, Int. Commun. Heat Mass Transfer 35 (6) (2008) 696–703, https://doi.org/10.1016/j.icheatmasstransfer.2008.02.002.

[24] B.K. Saha, J.I. Jihan, Md.Z. Ahammad, G. Saha, S.C. Saha, Enhanced thermal performance and entropy generation analysis in a novel cavity design with circular cylinder, Heat Transfer (2024), https://doi.org/10.1002/htj.22999.

[25] A.K. Singh, S. Roy, T. Basak, Analysis of Entropy Generation Due to Natural Convection in Tilted Square Cavities, IndraStra Global 51 (40) (2012) 13300–13318, https://doi.org/10.1021/ie3013665.

[26] M. Magherbi, H. Abbassi, A. Ben Brahim, Entropy generation at the onset of natural convection, Int. J. Heat. Mass Transf. 46 (18) (2003) 3441–3450, https://doi.org/10.1016/S0017-9310(03)00133-9.

[27] J.H. Saboj, P. Nag, G. Saha, S.C. Saha, Entropy Production Analysis in an Octagonal Cavity with an Inner Cold Cylinder: a Thermodynamic Aspect, Energies. (Basel) 16 (14) (2023) 5487, https://doi.org/10.3390/en16145487 (Basel).

[28] S.M. Seyyedi, A.S. Dogonchi, M. Hashemi-Tilehnoee, Z. Asghar, M. Waqas, D. D. Ganji, A computational framework for natural convective hydromagnetic flow via inclined cavity: an analysis subjected to entropy generation, J. Mol. Liq. 287 (2019) 110863, https://doi.org/10.1016/j.molliq.2019.04.140.

[29] F. Corvaro, M. Paroncini, A numerical and experimental analysis on the natural convective heat transfer of a small heating strip located on the floor of a square cavity, Appl. Therm. Eng. 28 (1) (2008) 25–35, https://doi.org/10.1016/j.applthermaleng.2007.03.018.